Environmental Science and Pollution Research (2019) 26:11012–11028
https://doi.org/10.1007/s11356-019-04522-6

RESEARCH ARTICLE

Long-term observation of cyanobacteria blooms using multi-source satellite images: a case study on a cloudy and rainy lake

Meng Mu[1,2] · Chuanqing Wu[3] · Yunmei Li[1,2] · Heng Lyu[1,2] · Shengzhong Fang[4] · Xiang Yan[4] · Ge Liu[5] · Zhubin Zheng[6] · Chenggong Du[1,2] · Shun Bi[1,2]

Received: 28 September 2018 / Accepted: 6 February 2019 / Published online: 21 February 2019

Abstract

High-frequency and reliable data on cyanobacteria blooming over a long time period is crucial to identify the outbreak mechanism of blooms and to forecast future trends. However, in cloudy and rainy areas, it is difficult to retrieve useful satellite images, especially in the rainy season. To address this problem, we used data from the HJ-1/CCD (Chinese environment and disaster monitoring and forecasting satellite/charge coupled device), GF-1/WFV (Chinese high-resolution satellite/wide field of view), and Landsat-8/OLI (Operational Land Imager) satellites to generate a time series of the bloom area from 2009 to 2016 in Dianchi Lake, China. We then correlated the responses of bloom dynamics to meteorological factors. Several findings can be drawn: (1) a higher bloom frequency and a larger bloom area occurred in 2011, 2013, and 2016, compared to the other years; (2) the frequency of blooms peaked in April, August, and November each year and expanded from north to south starting in July; (3) air temperature in spring and sunshine hours in summer greatly correlated to the yearly bloom area; (4) wind speed and sunshine hours strongly affected the short-term expansion of blooms and thereafter influenced the monthly bloom scale; and (5) rainfall had a strong short-term influence on the occurrence of blooms. Cyanobacteria blooms often occurred when wind speeds were less than 2.35 ± 0.78 m/s in the dry season and 2.01 ± 0.75 m/s in the rainy season, when there were 48 to 72 h of sunshine in the dry season and 35 to 57 h of sunshine in the rainy season, and when there was more than 10 mm of daily precipitation.

Keywords Dianchi Lake · Cyanobacteria bloom · Multi-source remote sensing image · Meteorological factors · Multi-timescales

Responsible editor: Vitor Manuel Oliveira Vasconcelos

✉ Yunmei Li
liyunmei@njnu.edu.cn

[1] Key Laboratory of Virtual Geographic Environment of Education Ministry, Nanjing Normal University, Nanjing 210023, China

[2] Jiangsu Center for Collaboration Invocation in Geographical Information Resource Development and Application, Nanjing 210023, China

[3] Satellite Environment Application Center, Ministry of Environmental Protection, Beijing 100029, China

[4] Kunming Environment Monitor Center, Kunming 650032, China

[5] Northeast Institute of Geography and Agricultural Ecology, Chinese Academy of Science, Changchun 130102, China

[6] School of Geography and Environmental Engineering, Gannan Normal University, Ganzhou 341000, China

Introduction

The excessive release of nutrients accelerates eutrophication in lakes and reservoirs; as a result, blooms are a growing threat in freshwater systems (Carmichael 2001; Heisler et al. 2008; Ho et al. 2017). Generally speaking, the phenomenon in which phytoplankton forms floating scums on the water surface is referred to as a bloom. After the blooms have been reported in the scientific literature for about 140 years in Alexandrina Lake (Francis 1878), the incidence and intensity of blooms have increased consistently around the world (Brand and Compton 2007; Zhou and Zhu 2006). Eutrophic lakes suffering from severe blooms can be found in different locations, with different meteorological backgrounds and land use conditions, such as Taihu Lake (Hu et al. 2010; Huang et al. 2015; Qin et al. 2007), Dianchi Lake (Huang et al. 2014; Sheng et al. 2012), and Chaohu Lake (Shi et al. 2013) in China; Lake Erie (Allinger and Reavie

2013; Ho et al. 2017; Stumpf et al. 2012) in North America; Lake Trummen in Sweden (Cronberg et al. 1981); and Lake Ontario in Canada (Higgins et al. 2012). The conditions in these lakes influence the start/end time, frequency, and severity of blooms. However, to reveal the causes of blooms, it is necessary to observe the occurrence of blooms over a long time period. Thus, a long-period reliable bloom record with a high frequency of samples is essential to identify the outbreak mechanism and forecast future trends.

Satellite remote-sensing technology is an effective means for long-period observation as it provides spatial and temporal data series, such as the changes in the concentration of total suspended matter, phycocyanin, chlorophyll-a (Shi et al. 2015a; Shi et al. 2015b; Zheng et al. 2015). Due to the characteristics of satellite remote-sensing images, the dynamic change of blooms can be depicted quickly and efficiently. Some studies have successfully derived long-term bloom records. For example, Ho et al. (2017) extended the historical bloom record of Lake Erie using Landsat images. Hu et al. (2010) described bloom patterns in Taihu Lake between 2000 and 2008. Huang et al. (2014) observed cyanobacteria blooms of Dianchi Lake via Landsat images from 1974 to 2009. Among the previous studies, several indices have been used to extract the area of blooms for inland lakes, including the normalized difference vegetation index (NDVI) (Kutser 2009), the enhanced vegetation index (EVI) (Lu et al. 2017), the floating algae index (FAI) (Hu et al. 2010; Kutser 2009; Shi et al. 2017; Zhang et al. 2016), virtual-baseline floating macroalgae height (VB-FAH) (Xing and Hu 2016), the cyanobacteria index (CI) (Ho et al. 2017; Stumpf et al. 2016; Stumpf et al. 2012), and fluorescence line height (FLH) (Huang et al. 2014).

Dianchi Lake is the largest lake on the Yungui Plateau in China, with a water coverage area of 294.21 km^2. The lake has suffered from severe eutrophication since the 1980s and has been affected by cyanobacteria blooms since 1989 (Huang et al. 2014). The weather of Dianchi Lake can be divided into dry (November to April) and rainy (May to October) seasons. In the rainy season, the sky is often covered by thick clouds, which makes it difficult to get enough clear satellite images to observe the cyanobacteria bloom. However, the uncertainty of bloom evaluation increases if there is a lack of long-term historical data (Bertani et al. 2016; Stumpf et al. 2016). Therefore, the present study tries to combine several different satellite images to increase the amount of data. Due to the area limitation of Dianchi Lake and the highly dynamic changes of the bloom, high spatial resolution image data are preferred (Davis et al. 2007; Li et al. 2015). In this study, images from the Landsat-8/OLI (Operational Land Imager), HJ-1/CCD (Chinese environment and disaster monitoring and forecasting satellite/charge coupled device), and GF-1/WFV (Chinese high-resolution satellite/wide field of view) satellites were used to analyze the cyanobacteria blooms from 2009 to 2016 in Dianchi Lake. The objectives of the present study were (1) to generate a long-term, reliable and frequent record of blooms in Dianchi Lake based on multi-source satellite images and (2) to determine the response of blooms to meteorological factors at various time scales.

Material and methods

Study area

Dianchi Lake is a plateau lake located between 24° 01′ N–24° 01′ N and 102° 36′ E–102° 47′ E (Fig. 1) near Kunming City, China. It is characterized by a semi-closed, wind-driven, low-latitude, and monsoon climate. The lake is 40.4 km long from south to north and 7 km wide from east to west, with a mean water depth of 4.4 m. Dianchi Lake was separated into two parts by Haigeng Dam in 1996. The north region is named Caohai, with an area of 7.43 km^2, while the south part is called Waihai, with an area of 286.78 km^2, occupying more than 97% of Dianchi Lake. Because Caohai has become a dead space with low water flow and high pollution (Pan et al. 2006), our study area specifically refers to Waihai (hereafter, Dianchi Lake specifically refers to Waihai). More than 20 tributaries run through Kunming City and empty into the lake, bringing a lot of urban wastewater. Especially in the rainy

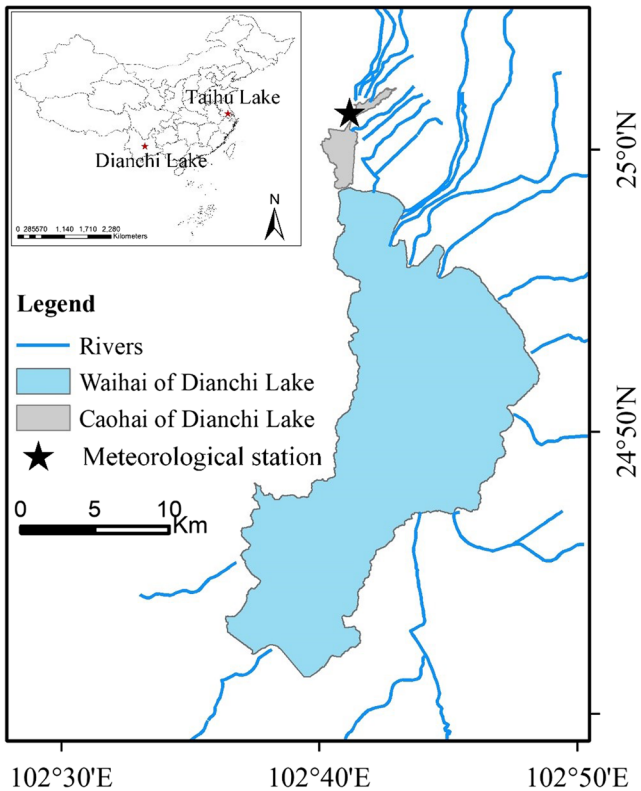

Fig. 1 Location of Dianchi Lake, the largest lake in Yunnan Province. The gray area is Caohai, the blue area is Waihai, and the blue lines are the rivers that flow into Dianchi Lake

season, a large amount of municipal and agricultural sewage is discharged into the lake. With the accumulation of pollutants year by year, the eutrophication of Dianchi Lake has become increasingly serious (Gao et al. 2005; Huang et al. 2018; Wu et al. 2018). Cyanobacteria blooms, which are the direct consequence of eutrophication, have occurred almost every year since 1989 (Huang et al. 2014).

Meteorological data

Air temperature (AT: °C), wind speed (WS: m/s), atmospheric pressure (PRS: hPa), precipitation (Pre: mm), and sunshine hours (SHs: h) at daily, monthly, and yearly timescales were obtained from meteorological station #56778 of the China Meteorological Administration (http://data.cma.cn) (Fig. 1).

Image data preprocessing

Landsat-8/OLI, GF-1/WFV, and HJ-1/CCD images from 2009 to 2016 were collected in this study. Landsat-8 was launched in 2013 and is the eighth satellite in the Landsat program. The OLI sensor on Landsat-8 has a spatial resolution of 30 m and a temporal resolution of 16 days. HJ-1 was launched in 2008 by China and consists of two satellites: HJ-1A and HJ-1B. Their combination can offer a 2-day revisit frequency. GF-1 was launched in 2013 by China, and it is equipped with four WFV sensors. It has a temporal resolution of 4 days when the four sensors are combined. The primary parameters of the three sensors are listed in Table 1.

GF-1/WFV and HJ-1/CCD images were downloaded from the China Centre for Resources Satellite Data and Application (CRESDA) website (http://www.cresda.com/ site1/), while the Landsat-8/OLI images were downloaded from the USGS Earth Explorer website (http://earthexplorer.usgs.gov/). The online thumbnail images were first visually examined, and then those with minimal cloud cover were chosen and downloaded. Table 2 shows the total number of images, with the number of blooms inside parentheses. There were 30 OLI images, 49 WFV images, and 408 CCD images from 2009 to 2016, including some images from different sensors on the same day. Thus, a total of 487 images were available, and 152 images were found to show cyanobacteria blooms.

The images were processed in two steps: radiometric calibration and quick atmospheric correction (Ho et al. 2017) in ENVI 5.3 software. In addition, the CCD and WFV images were geometrically corrected by referring to a fixed Landsat-8/OLI image using the nearest-neighbor approach, with RMSE within half of a pixel. The GF-1/WFV images were also resampled to 30 m spatial resolution.

Table 1 Characterizations of Landsat-8/OLI, GF-1/WFV, and HJ-1/CCD

Characterization	Landsat-8/OLI	GF-1/WFV	HJ-1/CCD
Operational period	2013 to present	2013 to present	2008 to present
Revisit period	16 days	4 days	2 days
Spatial resolution	30 m	16 m	30 m
Swath (km)	185	200 (1 WFV)	360 (1 CCD)
		800 (4 WFV)	700 (2 CCD)
Quantization	12 bits	10 bits	8 bits
Spectral bands (μm)	B1, 0.43–0.45		
	B2, 0.45–0.52	B1, 0.45–0.52	B1, 0.45–0.52
	B3, 0.52–0.60	B2, 0.52–0.59	B2, 0.52–0.60
	B4, 0.63–0.68	B3, 0.63–0.69	B3, 0.63–0.69
	B5, 0.84–0.89	B4, 0.77–0.89	B4, 0.76–0.90
	B6, 1.56–1.66		
	B7, 2.10–2.30		
	B9, 1.36–1.39		

Cyanobacteria bloom area retrieval

VB-FAH and thresholds of bloom area retrieval

The cyanobacteria bloom is defined as a collection of algae floating on the water surface that can be detected by remote sensing images in this study. A variety of indices have been successfully applied to the extraction of bloom information (Ho et al. 2017; Huang et al. 2014; Shi et al. 2017; Stumpf et al. 2016; Stumpf et al. 2012; Xing and Hu 2016; Zhang et al. 2016). Among them, the VB-FAH index uses the green and red bands as the baseline to measure the height of the near-infrared (NIR) reflectance. This is suitable for the spectral bands of Landsat-8/OLI, HJ-1/CCD, and GF-1/WFV. Xing and Hu (2016) also indicate that this index is not sensitive to interference from reflections and aerosols. Thus, considering the thick aerosols and thin clouds in the rainy seasons of Dianchi Basin, the VB-FAH index was used in this study to extract the bloom area. VB-FAH was calculated as follows:

$$VB{-}FAH = (\rho_{NIR}{-}\rho_{Green}) + (\rho_{Green}{-}\rho_{Red})*(\lambda_{NIR}{-}\lambda_{Green})/(2\lambda_{NIR}{-}\lambda_{Red}{-}\lambda_{Green}) \quad (1)$$

where ρ is the reflectance and λ is the wavelength, with the subscript representing the band of satellite sensors.

It is difficult to determine a threshold to separate the bloom pixels and non-bloom pixels due to the mixed pixels and observation geometry, and any choice of a fixed threshold will be a compromise, which will cause the bloom area data deviation (Xing and Hu 2016). In order to extract the bloom area accurately, this study determined the threshold of bloom identification by observing the bimodal histogram of VB-FAH in each image. Figure 2 shows an example of the VB-FAH frequency distributions of HJ-1/CCD, GF-1/WFV, and Landsat-8/OLI on 10 October 2013, 5 December 2016, and 2 August

Table 2 Number of Landsat-8/OLI, GF-1/WFV, and HJ-1/CCD images, with the number of images containing blooms in parentheses

Year	2009	2010	2011	2012	2013	2014	2015	2016	Total
OLI	***	***	***	***	7 (3)	8 (1)	9 (2)	6 (6)	30 (12)
WFV	***	***	***	***	8 (4)	18 (4)	13 (4)	10 (5)	49 (17)
CCD	63 (35)	56 (17)	63 (19)	83 (10)	51 (22)	48 (8)	25 (6)	19 (6)	408 (123)
Total	63 (35)	56 (17)	63 (19)	83 (10)	66 (29)	74 (13)	47 (12)	35 (17)	487 (152)

*** indicates there were no satellite images

2016. The curves of various sensors in Fig. 2 exhibited irregular doublet; the left part was a non-bloom area and the right part was a blooming area. Thus, for bloom pixels, the VB-FAH value was > 0.00 in HJ-1/CCD, > − 0.01 in GF-1/WFV, and > − 0.005 in the Landsat-8/OLI image.

Accuracy verification

Ideally, the extraction of the bloom area was evaluated by the concurrent ground truth data, but it is difficult in obtaining the concurrent ground truth data for mixed pixels and observation geometry (Hu et al. 2010; Kutser 2004). Thus, the accuracy of bloom area extraction was evaluated by comparing the extracted results with visual interpretation and using VB-FAH methods at the boundary of the bloom and non-bloom areas. As an example, Fig. 3 shows a region in Dianchi Lake with false-color composite images from Landsat-8/OLI, GF-1/WFV, and HJ-1/CCD; bloom extraction results by visual interpretation; and bloom extraction results by VB-FAH. Assuming the visual interpretation is accurate, the overall accuracy (defined as the ratio of the number of category pixels correctly classified to the total number of categories) of VB-FAH is 96.99% for Landsat-8/OLI, 90.69% for HJ-1/CCD, and 91.54% for GF-1/WFV. This indicates that VB-FAH is suitable for cyanobacteria bloom extraction in Dianchi Lake.

Consistency of bloom area retrieval by different sensors

Table 1 shows the instrument features of LC-8/OLI, HJ-1/CCD, and GF-1/WFV, which have several differences. The difference must be taken into consideration when they were used jointly. The first major difference lies in the discrepancy of the spectral response function between the three sensors (Fig. 4), along with typical R_{rs} of case II water and blooming water as references. WFV and CCD have a wider spectral response in the NIR band compared with the corresponding band of OLI, which will affect the spectral sensitivity of the signals. However, bloom pixels have a stronger signal than bloom-free water pixels, especially in the NIR band (the R_{rs} curve of the bloom has a significant rise in the NIR band), so the two sensors can still receive enough signals (Li et al. 2015). The second major difference lies on the quantization level which is 12 bits of OLI, 10 bits of WFV, and 8 bits of CCD. Although CCD was the lowest, it has been successfully adopted to detect blooms (Cui et al. 2012). So the ability of the sensors to identify bloom pixels is unquestionable. Thus, we only need to consider the consistency of the bloom area products. Two pairs of concurrent images over Dianchi Lake were used to study the consistency in their retrieval of the bloom area. HJ-1/CCD and GF-1/WFV images were acquired on 8 November 2013, 43 min apart, and HJ-1/CCD and Landsat-8/OLI images were acquired on 28 July 2014, 44 min apart.

Comparison between HJ-1/CCD and GF-1/WFV The bloom area derived from HJ-1/CCD was 12.1833 km^2, while it was 12.6927 km^2 from GF-1/WFV; thus, there was a slight discrepancy between the two sensors.

Figure 5 shows the bloom area extracted by the two sensors in the northern part of the lake. 2.1717 km^2 of bloom area was detected by the HJ-1/CCD but not by the GF-1/WFV image, while 1.6434 km^2 of area was detected by the GF-1/WFV but not by the HJ-1/CCD image.

The discrepancy in the bloom area between the two sensors was mainly caused by weather conditions. Although the mean wind speed was 2.4 m/s, the maximum was 5 m/s on 8 November 2013. That may have led to the horizontal and

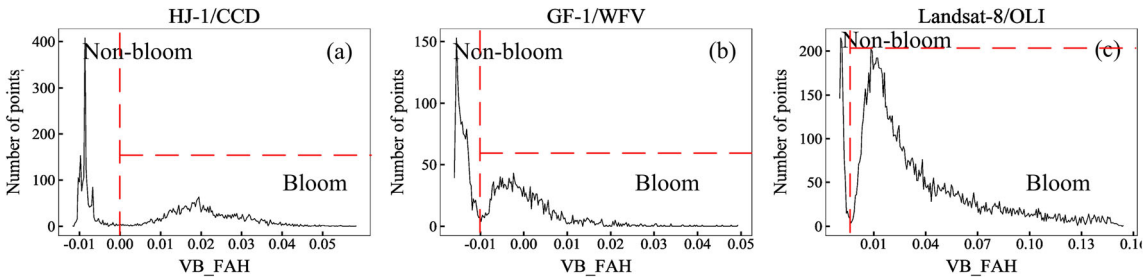

Fig. 2 Frequency distributions of VB-FAH from different satellite sensors over a small region of Dianchi Lake, including both blooming area and non-bloom area. **a** HJ-1/CCD on 10 October 2013, **b** GF-1/WFV on 5 December 2016, **c** Landsat-8/OLI on 2 August 2016

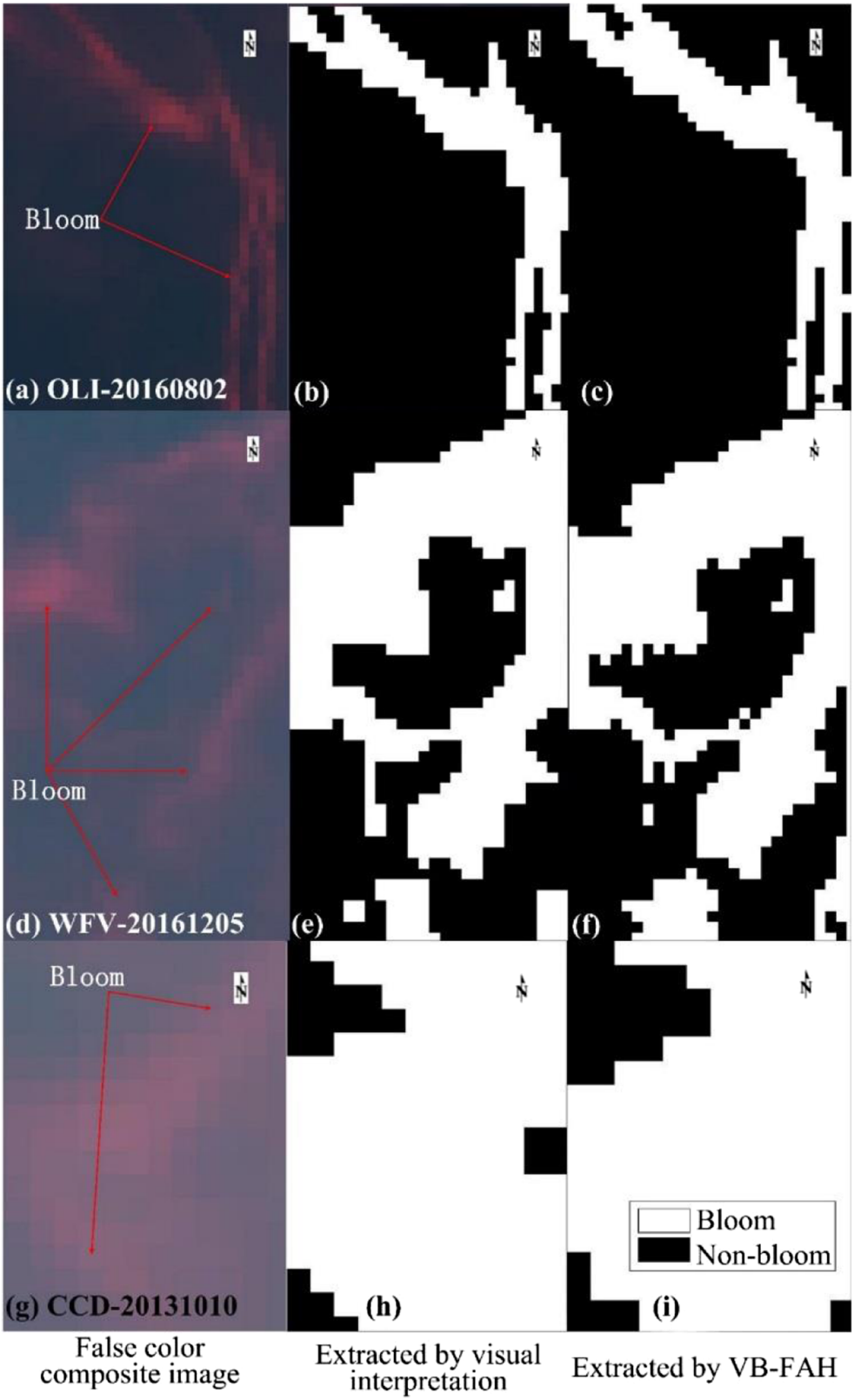

Fig. 3 Comparing results of blooms extracted by visual interpretation and VB-FAH. **a**, **d**, **g** False-color composite images; the dark red pixels represent blooms. **b**, **e**, **h** The results extracted by visual interpretation. **c**, **f**, **i** The results extracted by VB-FAH. The white and black areas represent bloom pixels and non-bloom pixels, respectively

vertical movement of the bloom (Cao et al. 2006; Hu et al. 2010; Ma et al. 2015). In addition, the wind blew from the southwest on 8 November 2013, which may have caused the bloom patches to move to the northeast. The purple pixels in Fig. 5c indicate that the bloom did indeed move to the northeast in the GF-1/WFV image.

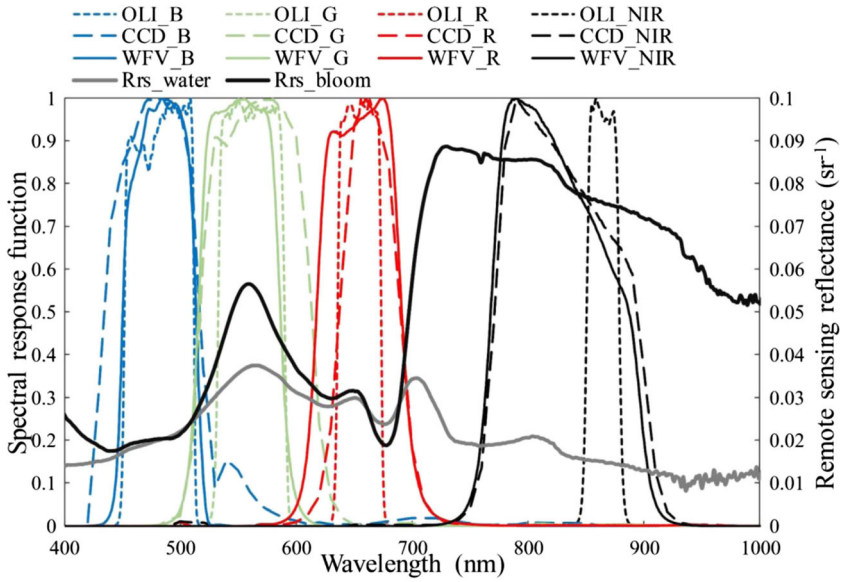

Fig. 4 The spectral response function of Landsat-8/OLI (short dashed lines), HJ-1/CCD (long dashed lines), and GF-1/WFV (solid lines), along with typical R_{rs} of case II water and blooming water as references

Despite the slight discrepancy, the relative error was only 0.5094 km^2 between the two bloom areas. It only accounted for 5.69% of the bloom area (the green area in Fig. 5c) which was commonly detected by the two sensors; thus, the bloom areas derived from HJ-1/CCD and GF-1/WFV are consistent and comparable and can be combined for the long-term monitoring of blooms.

Comparison between Landsat-8/OLI and HJ-1/CCD The bloom area derived from HJ-1/CCD on 28 July 2014 was 123.3378 km^2, while it was 111.3147 km^2 from Landsat-8/OLI; thus, there was a slight discrepancy between the two sensors.

Figure 6 shows the spatial distribution of the cloud and bloom extracted by the two sensors. 24.2467 km^2 of bloom area was detected by HJ-1/CCD that disappeared in the Landsat-8/OLI image, while 14.2236 km^2 of bloom area was detected by Landsat-8/OLI and not by HJ-1/CCD. The purple pixels in Fig. 6c represent the bloom area only found in the Landsat-8/OLI image, which was taken 44 min after the HJ-1/CCD image. The yellow color indicates bloom pixels that were only found in the HJ-1/CCD image. Comparing the two, the moving trace appears to have moved from the northeast to the southwest, which is consistent with the wind direction on 28 July 2014. The thin cloud can also be seen in the Landsat-8/OLI image (Fig. 6b, purple and yellow rectangles), which may have caused the deviation in bloom area extraction.

Thus, the bloom areas derived from HJ-1/CCD, GF-1/WFV and Landsat-8/OLI are consistent and comparable and can be combining to monitor dynamic changes in blooms.

Results and analysis

Yearly distribution of cyanobacteria blooms in Dianchi Lake

Cyanobacteria bloom area was retrieved using the multi-source satellite images from 2009 to 2016. The start/end date and frequency of bloom, and the average and maximum bloom area, are shown in Table 3. Usually, the bloom began

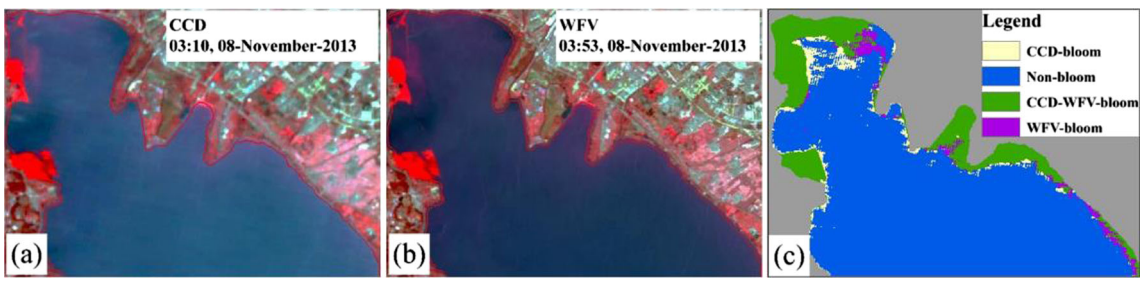

Fig. 5 Comparison of the bloom area derived from HJ-1/CCD and GF-1/WFV on 8 November 2013. **a** False-color composite image by WFV. **b** False-color composite image by CCD. **c** Comparison of the extracted bloom area of the two sensors. Non-bloom, non-bloom water for both sensors; CCD-WFV-bloom, bloom water for the two sensors; CCD-bloom, bloom water by CCD but non-bloom by WFV; WFV-bloom, bloom water by WFV but non-bloom by CCD

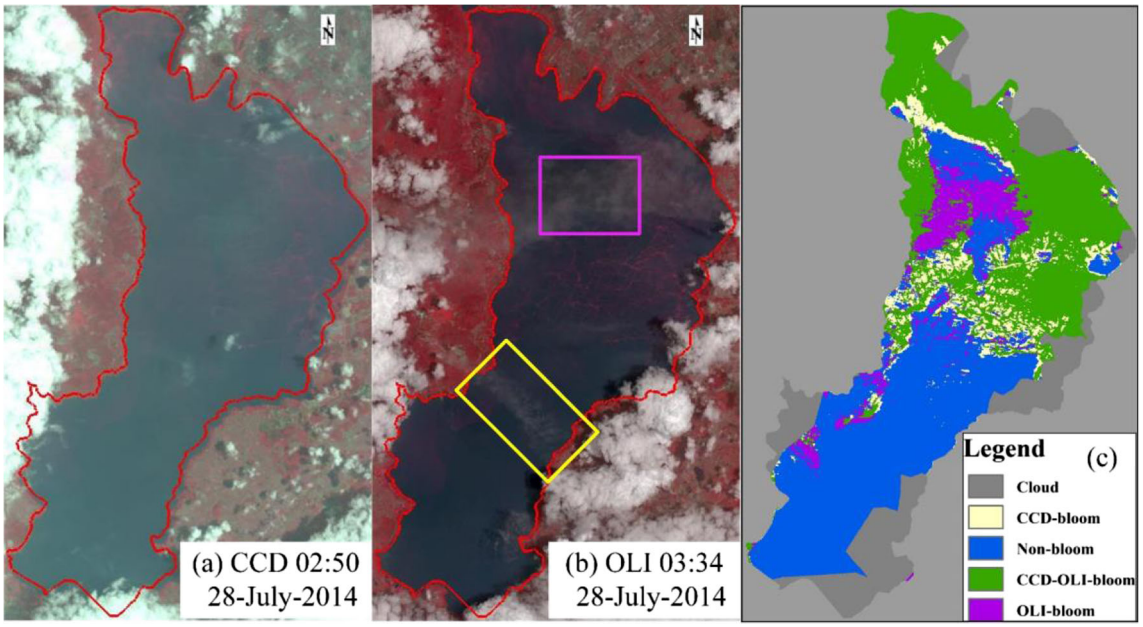

Fig. 6 Bloom area comparison derived from HJ-1/CCD and Landsat-8/OLI on 28 July 2014. **a** False-color composite image by CCD. **b** False-color composite image by OLI. **c** Comparison of the extracted bloom area of the two sensors. Non-bloom, non-bloom water for the two sensors; CCD-OLI-bloom, bloom water for the two sensors; CCD-bloom, bloom water by CCD but non-bloom by OLI; OLI-bloom, bloom water by OLI but non-bloom by CCD

in March/April and ended in December, according to the available images, except in 2016. In 2016, the bloom was not observed until July 25th, due to the fact that the images are blocked by clouds from March to June, making it impossible to know the starting time. The area of the bloom in each image is presented in Fig. 7. The greatest areas, which suggest the most serious blooms, occurred in 2011, 2013, and 2016. In those years, the maximum bloom area occupied more than 50% of the total area. The smallest bloom area was 45.8658 km^2 and occurred in 2009, occupying 15.99% of the total area. It is worth mentioning that, although there was not a large bloom area and the area of most blooms was less than 20 km^2, the bloom frequency was very high in 2009. In addition, although the extent of the bloom showed an alternating trend over the years, the maximum bloom area extended from 2009 to 2016, whether in blooming years (2011, 2013, and 2016) or in non-blooming years (2009, 2010, 2012, 2014 and 2015).

Monthly distribution of cyanobacteria blooms in Dianchi Lake

The average and maximum area and the frequency of blooms are presented in Fig. 8. The bloom frequency of Dianchi Lake followed a "three peaks" phenomenon, and no blooms were observed in January and February during the period of investigation. Therefore, the blooms in Dianchi Lake can be classified into two periods. The first period is from March to June, with the first peak appearing in April; the frequency is low and most bloom areas were less than 20 km^2 in this period. The second period is from July to November. During this period, cyanobacteria blooms occurred heavily, with two peaks in August and November, respectively. In addition, bloom frequency and size both reached the highest of the year in this period.

The finding of two peaks in spring and autumn in this study extended the discovery of previous research on Dianchi Lake (Sheng et al. 2012), in which only one peak was observed between June and September. The phenomenon of a peak appearing in autumn was similar to Lake Erie, where one peak occurred in August and another in late September in 2016 (Stumpf et al. 2012).

Spatial distribution of cyanobacteria blooms

Spatially, the blooms were concentrated in the northern part of the lake, but they had a slight tendency to extend to the south. The same situation was observed by Huang et al. (2014), whose study showed that blooms in Dianchi Lake spatially occurred from north to south from the late 1980s to the early 1990s. The area suffering from blooms extended almost one fourth of the length from north to south in 2009, but it stretched to more than one half of the length of the lake in 2016. As an extreme example, on July 25, 2016, the bloom covered the entire lake.

The bloom frequency of each pixel with 30 m spatial resolution was calculated using the 487 images, and the spatial variability is shown in Fig. 9. The frequency of each pixel

Table 3 Statistics of blooms from 2009 to 2016

Year	Starting date yyyy-mm-dd	End date yyyy-mm-dd	Average bloom Area (km^2)	Maximum bloom Area (km^2)	Bloom Frequency
2009	2009-03-09	2009-12-13	12.91	45.8658	55.56%
2010	2010–03-21	2010–12-21	25.86	67.0977	30.36%
2011	2011–04-02	2011–12-20	52.78	149.0589	30.16%
2012	2012-03-20	2012-12-21	29.44	65.9997	12.05%
2013	2013-03-09	2013-12-20	41.69	156.9501	48.28%
2014	2014-04-20	2014-12-29	20.51	86.3055	20.34%
2015	2015-04-20	2015-11-24	25.62	74.1042	26.19%
2016	2016-07-25	2016-12-08	49.79	165.3093	48.39%

Note: the bloom frequency is the percentage of images with blooms in total images

ranged from zero to 55.56%. The higher values were in the northern part, while the lower values were in the central and southern areas of the lake. Generally, about 35,917 pixels suggested blooms in a year. However, in the heavy bloom years, such as 2011, 2013, and 2016, the number of bloom pixels increased to more than 50,000 pixels, and the frequency increased over almost the entire lake.

To study the spatial distribution in different seasons, the frequency of the occurrence of the bloom was counted in each month (Fig. 10). Consistent with the above analysis, the northern lake experienced more blooms in all months (excluding January and February). Blooms first occurred in the northern region in March, then the coverage extended to the southern lake starting in July, and then to the entire lake. The high frequency of blooms lasted from July to November, then gradually decreased in December and completely disappeared in January.

Discussion

Advantages of combining satellite sensor data

Because of the cloudy and rainy weather in Dianchi Lake, it is difficult to get satellite images with a clear sky. For example, although HJ-1 is a high temporal resolution satellite with a revisit period of two days, there are fewer cloud-free images, especially in the rainy season. In 2016, only 19 images could be used. The lack of data has been an obstacle to long-term monitoring of blooms in Dianchi Lake.

The combination of the three satellite sensors greatly increases the available image numbers for the long-term monitoring of blooms. From 2013 to 2016, there were 30 effective images from Landsat-8/OLI, 49 from GF-1/WFV, and 408 from HJ-1/CCD. Consequently, the opportunity for bloom detection increased due to the total of 455 images (Only one image was reserved when several images were acquired in the same day. Thus, 32 images were deleted, and the deletion order is HJ-1/CCD, GF-1/WFV, and Landsat-8/OLI). Of particular interest are the 56 images that were acquired in the rainy season, which greatly decreases the revisit cycle and increases the monitoring frequency of bloom events.

By combining the three sensors, some dynamic changes in the bloom process were captured. One case is the development of a cyanobacteria bloom from October 10 to October 13 (named Case Oct, Fig. 11), in which the bloom area reached 109.94 km^2 on October 10, then reduced to 15.96 km^2 on October 13. In general, the dynamic process involves horizontal and vertical movement, accompanied by the growth and extinction of cyanobacteria. However, the rapid change in bloom area is mainly influenced by weather conditions, such as wind speed and pressure (Kahru et al. 1993; Shi et al. 2017; Wu et al. 2015; Zhang et al. 2016). To reveal the influence of weather conditions on blooms in Dianchi Lake, we analyzed the relationship between meteorological factors and blooms.

Relationship between cyanobacteria blooms and meteorological factors

There are two prerequisites for blooms: sufficient cyanobacterial cells and suitable weather conditions for promoting the cells to the water surface (Reynolds 2006). Previous studies have suggested that the accumulation and floatation of phytoplankton cells are highly correlated to weather conditions (Walsby 1994). However, which meteorological parameters are the most important for blooms in Dianchi Lake? Moreover, what is the influence of meteorological conditions on blooms? To answer these questions, we analyzed the relationships between bloom area and wind speed (WS), sunshine hours (SHs), pressure (PRS), air temperature (AT), and precipitation (Pre) from the perspective of the various timescales.

Relationship between cyanobacteria bloom and wind speed

Wind speed (WS) exhibits strong seasonal variability. The average wind speed is significantly lower in the rainy season

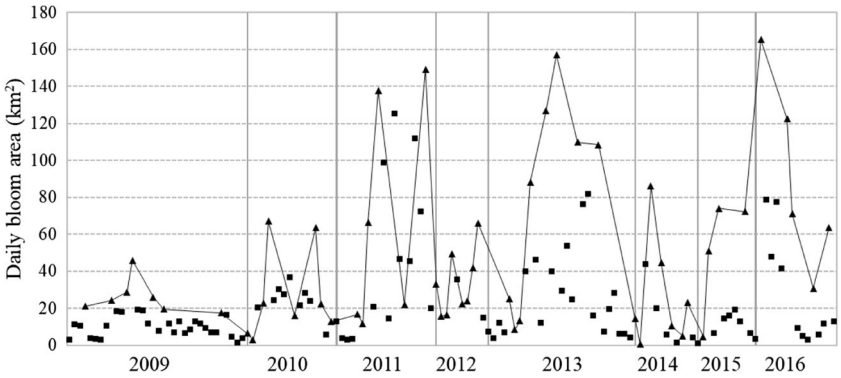

Fig. 7 Daily bloom coverage of Dianchi Lake derived from the combined images. The triangles represent the monthly maxima in bloom area and are connected by lines, and the different years are separated by the grey vertical lines

(2.21 ± 0.40 m/s) than in the dry season (2.99 ± 0.55 m/s). The daily average WS exhibits substantial variability, ranging from 0.30 to 8.60 m/s. Previous studies have indicated that strong wind affects the vertical movement of blooms and may lead to the disappearance of water surface blooms (Kahru et al. 1993; Shi et al. 2018; Wu et al. 2015). Hence, we analyze the relationship between blooms and wind speed at yearly, monthly, and daily scales.

Figure 12 shows that yearly average WS has a less significant negative correlation with yearly average bloom area ($r = -0.125$, $p = 0.768$). Thus, the interannual difference in WS does not explain the variations in yearly bloom intensity with the existing data set.

Figure 12b shows there was a significant negative correlation ($r = -0.586$, $p < 0.01$) between ln(monthly average bloom area) and monthly average WS. This indicates that the change in wind speed at the monthly scale has a significant impact on the bloom area. A similar result was obtained by Lu et al. (2017).

In order to study the relationship between blooms and short-term wind-speed change, we compared the mean wind speeds near the date the images were taken (Fig. 12c): the average WS on the day when the bloom was observed by satellite images (bloom day) (B0-1), the average WS on the day when no bloom was observed by satellite images (non-bloom day) (B0-0), the average WS on the day before the bloom day (B1-1), the average WS on the day before the non-bloom day (B1-0), the average WS on the day and the day before the bloom day (B1M-1), the average WS on the day and the day before the non-bloom day (B1M-0), the average WS on the day and the two days before the bloom day (B2M-1), and the average WS on the day and the two days before the non-bloom day (B2M-0).

The daily average WS on bloom days (B0-1) was significantly lower than that on non-bloom days (B0-0). Similarly, the mean WS on the day and two days before bloom days was lower than that of non-bloom days. It can be concluded that lower WS is beneficial to the formation of blooms. In addition, ln(daily bloom area) was strongly correlated with the daily average WS ($r = -0.365$, $p < 0.01$) (Fig. 12e). This indicates the bloom area contracted with increasing WS in Dianchi Lake, which is consistent with Xie et al. (2010) and Li et al. (2011). Li et al. (2011) suggested that a favorable WS for blooms in Dianchi Lake is less than 3 m/s. However, we discovered that the critical thresholds varied by season due to the strong division in WS between the dry and rainy seasons (the daily average WSs on bloom days were 2.35 ± 0.78 m/s in the dry season and 2.01 ± 0.75 m/s in the rainy season). The

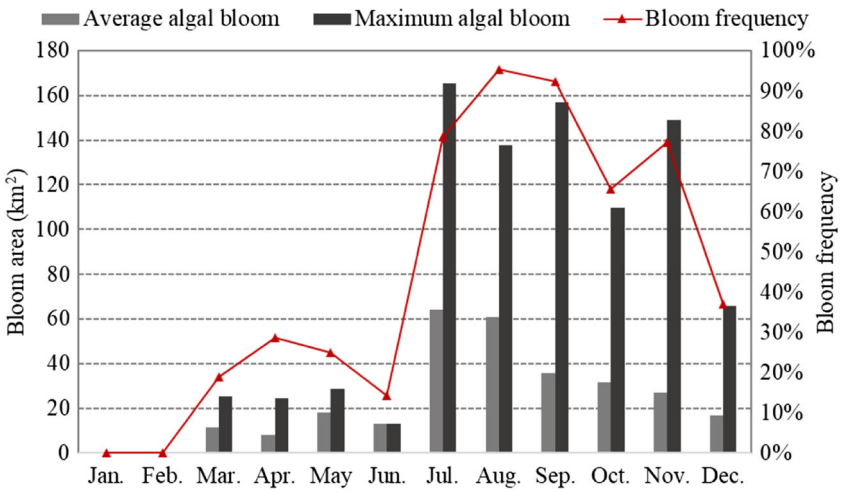

Fig. 8 Monthly bloom distribution of Dianchi Lake. Light and dark histograms represent the average and maximum areas of blooms in each month. The red triangles represent bloom frequency

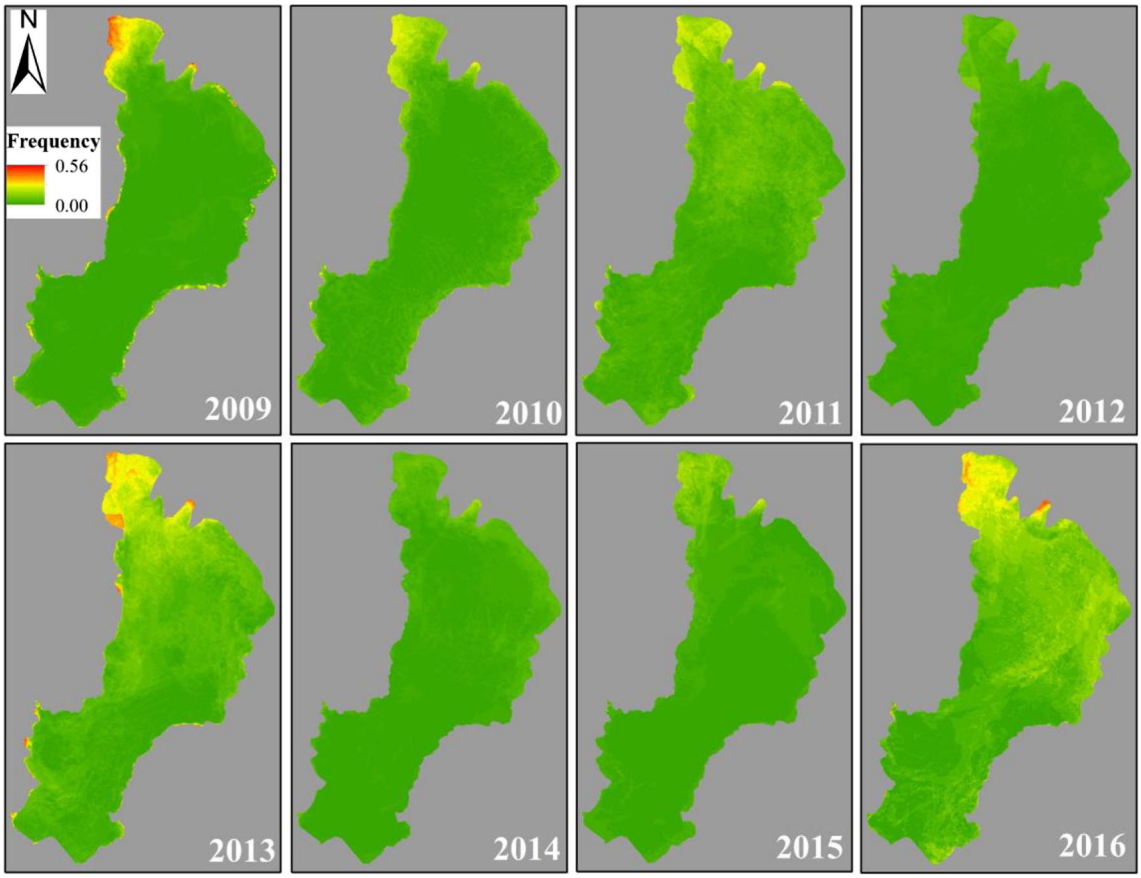

Fig. 9 Bloom frequency of pixels derived from 2009 to 2016 using 487 images

bloom event in Case Oct verified this result: the daily average WSs were 1.7 m/s, 1.2 m/s, 1.5 m/s, and 1.8 m/s from October 10 to October 13, which are favorable for blooms. In addition, the WS increased from October 11 to October 13, resulting in a decrease in bloom area.

In summary, monthly average WS and monthly average bloom area, as well as average daily WS and daily bloom area, exhibited statistically significant negative correlations. This indicates that relatively low WS facilitated the occurrence of blooms.

Relationship between cyanobacteria blooms and sunshine hours

Yearly sunshine hours (SHs) ranged from 2052.80 to 2636.40 h from 2009 to 2016 in Dianchi Lake, with an average of 2327.64 ± 223.55 h. The number of SHs is significantly lower in the dry season (230.73 ± 28.91 h) than in the rainy season (157.21 ± 40.66 h). The minimum monthly average number of SHs is in September, while the maximum is in March. Solar radiation is the energy source of algae growth and reproduction, and it is a necessary condition for biomass accumulation. Here, we analyze the relationship between blooms and SHs at yearly, monthly, and daily scales.

The yearly average bloom area is weakly correlated with yearly SHs ($r = -0.385$, $p = 0.346$). However, the yearly average bloom area exhibits a statistically significant positive correlation ($r = 0.737$, $p < 0.05$) with the sum of SHs in summer (Fig. 13a). Thus, blooming years (2011, 2013, 2016) may be caused by longer SHs in the summer; the interannual difference in summer SHs may explain the variations in yearly bloom intensity.

There was a significantly negative correlation ($r = -0.551$, $p < 0.01$) between ln(monthly average bloom area) and monthly SHs in Fig. 13b. This is consistent with Lu et al. (2017), but is inconsistent with studies of other lakes (Huisman and Sommeijer 2002; Zhang et al. 2012). In order to compare the difference, we obtained the sunshine patterns from Dongshan meteorological station #58358 at Lake Taihu (Fig. 1) from the China Meteorological Administration (http://data.cma.cn). The number of monthly SHs was significantly lower in the dry season (147.61 ± 42.23 h) than in the rainy season (189.83 ± 52.85 h) in Lake Taihu, which was contrary to that in Dianchi Lake from 2009 to 2016. This may be the reason why Lake Taihu has one bloom peak while Dianchi Lake has three. In addition, the ultraviolet radiation in Dianchi Lake is much higher because of the

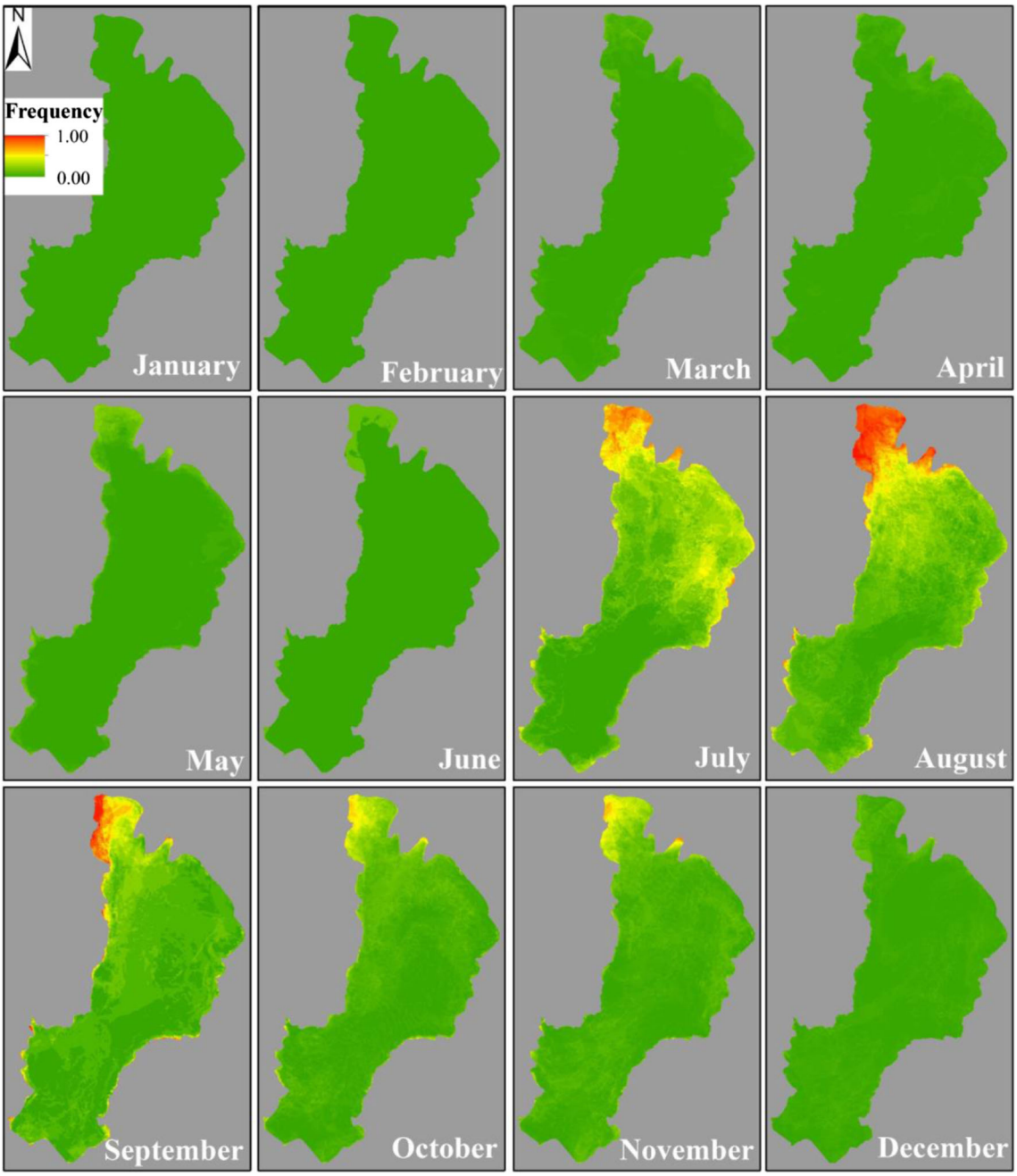

Fig. 10 Bloom frequency of pixels in each month derived from 2009 to 2016 using 487 images

high altitude (about 1888 km). From this, it can be inferred that the high number of SHs results in photoinhibition of algae (Gerla et al. 2011; Zhou et al. 2016). Hence, the accumulation of cyanobacteria may be inhibited in areas that experience strong light for a short period of time.

In order to study the relationship between blooms and change in short-term sunshine hours, we compared daily SHs near the date when the satellite images were taken (Fig. 13c): daily sunshine hours on the day when the bloom was observed by satellite images (bloom day) (B0-1), daily sunshine hours on the day when no bloom was observed by satellite images (non-bloom day) (B0-0), cumulative sunshine hours from the four days before the bloom day (B4S-1), cumulative sunshine hours from the four days before the non-bloom day (B4S-0), cumulative sunshine hours from the seven days before the bloom day (B7S-1), and cumulative sunshine hours from the seven days before the non-bloom day (B7S-0).

There is no difference between bloom days (B0-1) and non-bloom days (B0-0). However, cumulative SHs from the four/seven days before bloom days were lower than that of

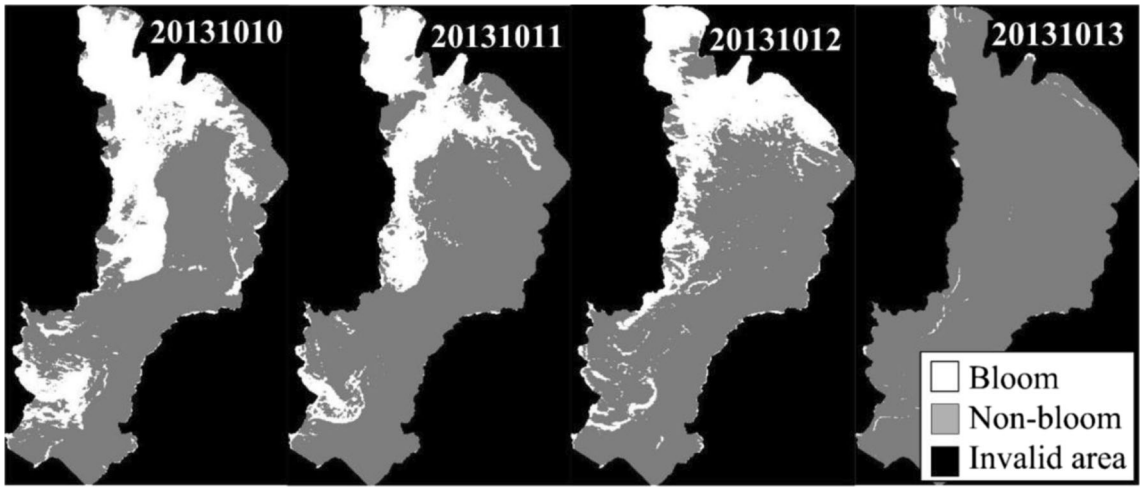

Fig. 11 A continuous bloom event monitored by multiple satellites, which depicted the decline of a bloom event

non-bloom days. In particular, when the cumulative SHs from the seven days before bloom days were between 48 and 72 h, it was beneficial to the bloom formation in the dry season, while suitable cumulative SHs were between 35 and 57 h in rainy season. It is worth mentioning that the sum of SHs from the seven days before October 10 to October 13 were 41.3 h, 48.7 h, 54.9 h, and 63.6 h, respectively (Case Oct). The gradual increase in SHs may also be one of the reasons for the disappearance of the bloom.

In summary, a higher number of SHs is beneficial for bloom formation in summer, but in other seasons, a lower number of SHs is favorable.

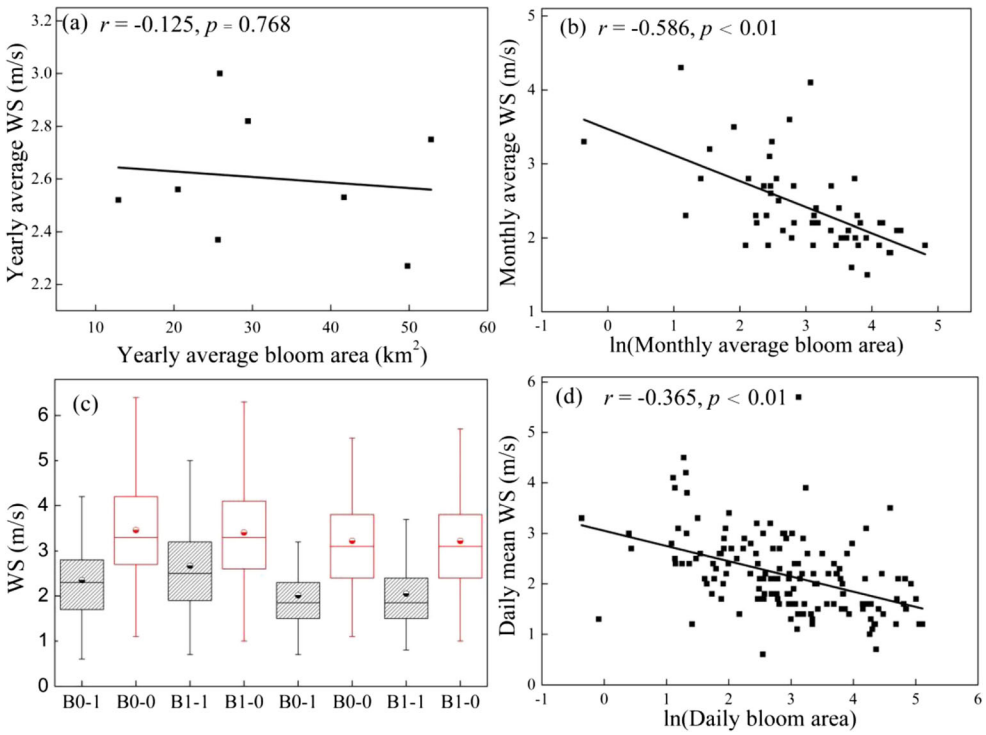

Fig. 12 Correlations between bloom area and wind speed at different time scales. **a** Yearly time scale; **b** monthly time scale; **c** box plot of short-term WS; **d** daily time scale. The black boxes represent the WSs relevant to bloom days and the red boxes represent the WSs relevant to non-bloom days. B0-1, the average WS on the day when the bloom was observed by satellite images (bloom day); B0-0, the average WS on the day when no bloom was observed by satellite images (non-bloom day); B1-1, the average WS on the day before the bloom day; B1-0, the average WS on the day before the non-bloom day; B1M-1, the average WS on the day and the day before the bloom day; B1M-0, the average WS on the day and the day before the non-bloom day; B2M-1, the average WS on the day and the first two days before the bloom day; B2M-0, the average WS on the day and the first two days before the non-bloom day

Relationship between cyanobacteria blooms and air temperature

Yearly air temperature (AT) exhibits a gentle change from 15.48 to 16.65 °C. The monthly average AT was 12.71 ± 4.14 °C in the dry season and 19.65 ± 2.53 °C in the rainy season. The daily average AT varied between − 3.3 and 25.6 °C, with an average of 16.19 ± 4.87 °C, and a daily average AT below 0 °C was very rare. AT is an important factor affecting algae particle growth and biomass accumulation. Here, we analyze the relationship between blooms and air temperature at yearly, monthly, and daily scales.

The yearly average bloom area is highly negatively correlated with yearly average AT ($r = -0.918$, $p < 0.01$). This indicates that temperature has a certain influence on the occurrence of blooms at the yearly scale. However, this does not conform with other research, since most studies have suggested that warm weather is suitable for the growth of blooms (JÖHnk et al. 2008; Kanoshina et al. 2003; Paerl and Huisman 2008). To further verify the relationship between temperature and blooms, we analyzed the correlations between the yearly average bloom area and the temperature of different seasons. The correlation coefficients for winter, spring, summer, and autumn were − 0.324 ($p = 0.434$), − 0.705 ($p = 0.050$), − 0.249 ($p = 0.550$), and − 0.524 ($p = 0.183$), respectively. A close negative correlation between yearly bloom area and AT in the spring was observed. This may be caused by the mechanism of generalized vernalization (low temperature promotes the reproduction of non-plant organisms) of *Microcystis aeruginosa* in Dianchi Lake (Guo et al. 2016; Guo et al. 2015). The negative correlation indicates that the low AT in spring has a great influence on blooms in Dianchi Lake.

However, the situation is different at a short timescale. ln(monthly average bloom area) and monthly average AT exhibited a less significant correlation ($r = 0.222$, $p = 0.110$). Thus, AT is not the main influencing factor for bloom formation at the monthly scale.

In order to validate the relationship between blooms and short-term air temperature change, we compared the average ATs near the date images were taken (Fig. 14): the average AT on the day when the bloom was observed by satellite images (bloom day) (B0-1), the average AT on the day when no bloom was observed by satellite images (non-bloom day) (B0-0), cumulative AT from the four days before the bloom day (B4S-1), cumulative AT from the four days before the non-bloom day (B4S-0), cumulative AT from the seven days before the bloom day (B7S-1), and cumulative AT from the seven days before the non-bloom day (B7S-0).

Figure 14 shows that there is no obvious difference between ATs on bloom days and non-bloom days. However, the medians of cumulative AT from the four/seven days before bloom days were slightly higher than that of non-bloom days in the dry season. Conversely, they were slightly lower than that of non-bloom days in the rainy season. This may explain the weak relationship between monthly blooms and AT. Similarly, there was a weak positive correlation between daily average AT and ln(daily bloom area) ($r = 0.260$, $p < 0.01$).

In summary, low AT in spring is beneficial for blooms, and daily mean AT slightly promotes the occurrence of blooms. Evidently, AT is not a key factor in bloom formation in Dianchi Lake.

Relationship between cyanobacteria bloom and pressure

Previous studies have suggested that lower pressure (PRS) promotes blooms (Cloern et al. 2005) by floating algae particles to the water surface (Carey et al. 2012; Zhang et al. 2016) through gas vesicles. However, from the data used in this study, PRS does not relate with yearly, monthly, or daily average PRS (the yearly scale: $r = 0.208$, $p = 0.621$; the monthly scale: $r = -0.095$, $p = 0.500$; the daily scale: $r = -0.022$, $p = 0.795$). This may be caused by only slight variation in PRS during the year, with a yearly average of 810 ± 0.62 hPa in Dianchi Lake. Dianchi basin is in an extremely low pressure state throughout the year, causing the algae particles to be insensitive to PRS. In addition, PRS in Dianchi Lake was much lower than in Lake Taihu (the yearly average PRS was 12,169.18 ± 6.42 hPa from 2009 to 2016 at meteorological station #58358). This may explain the different influence of PRS on blooms in Dianchi Lake compared to other lakes.

Relationship between cyanobacteria blooms and precipitation

Yearly precipitation (Pre) ranged from 565.80 to 1190.4 mm from 2009 to 2016 in Dianchi Lake, with an average of 889.99 ± 229.12 mm. There was an obvious division in Pre between the dry season (117.14 ± 70.45 mm) and rainy season (772.85 ± 186.85 mm). More than 85% of Pre occurred in the rainy season, and the maximum daily Pre reached 112.9 mm.

Previous studies have indicated that heavy rain will lead to a temporary increase of nutrients, which is beneficial for blooms (Shaw et al. 2001; Yang et al. 2016). Moreover, some studies have pointed out that a higher number of small rainfall events favor the proliferation of cyanobacteria (Reichwaldt and Ghadouani 2012). However, what is the influence of precipitation on blooms in Dianchi Lake? To answer this question, we explore the precipitation character and its relationship with bloom area at yearly, monthly, and daily scales.

The yearly average bloom area is very weakly correlated with yearly Pre ($r = 0.064$, $p = 0.880$). However, monthly Pre exhibited statistically significant positive correlation with monthly average bloom area ($r = 0.533$, $p < 0.01$). This indicates that Pre has a strong effect on blooms in the short term, but the influence declines at the yearly scale.

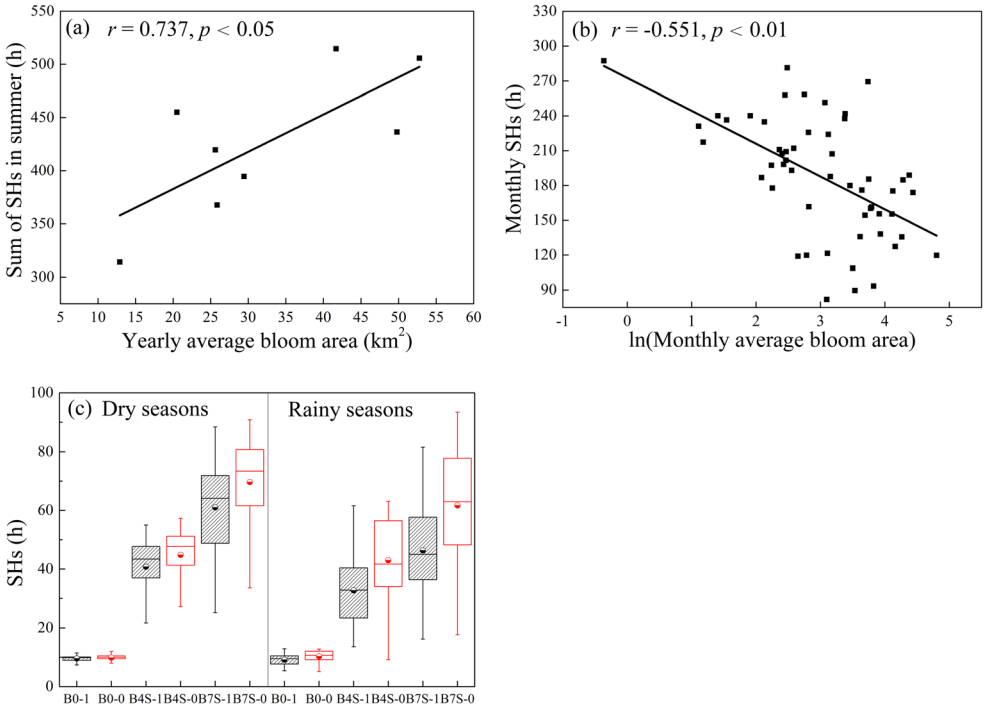

Fig. 13 Correlations between bloom area and sunshine hours at different time scales. **a** Season time scale at summer, **b** monthly time scale, **c** box plot of SHs in the short term. The black boxes represent the SHs relevant to bloom days, and the red boxes represent the SHs relevant to non-bloom days. B0-1, daily sunshine hours on the day when the bloom was observed by satellite images (bloom day); B0-0, daily sunshine hours on the day when no bloom was observed by satellite images (non-bloom day); B4S-1, cumulative sunshine hours from the four days before the bloom day; B4S-0, cumulative sunshine hours from the four days before the non-bloom day; B7S-1, cumulative sunshine hours from the seven days before the bloom day; B7S-0, cumulative sunshine hours from the seven days before the non-bloom day

In order to study the relationship between blooms and short-term Pre change, we compared the precipitation on days near the date the images were taken (Fig. 15): daily precipitation on the day when the bloom was observed by satellite images (bloom day) (B0-1), daily precipitation on the day when no bloom was observed by satellite images (non-bloom day) (B0-0), cumulative precipitation from the four days before the bloom day (B4S-1), cumulative precipitation from the four days before the non-bloom day (B4S-0), cumulative precipitation from the nine days before the bloom day (B9S-1), and cumulative precipitation from the nine days before the non-bloom day (B9S-0).

There was no difference in Pre between bloom days (B0-1) and non-bloom days (B0-0). Similarly, the cumulative Pre in the previous four/nine days before bloom days also had no difference with the before non-bloom days in the dry season. However, in the rainy season, the difference was significant. Moreover, our data show that the favorable accumulation of Pre from the nine days before a bloom day was more than 10 mm. It is worth mentioning that the sum of Pre from the

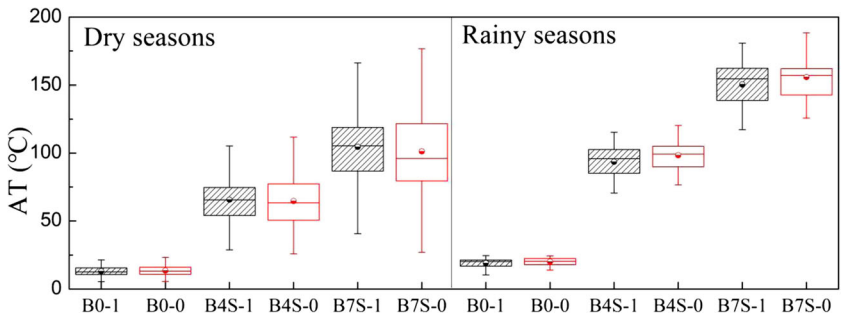

Fig. 14 Box plot of AT in the short term. The black boxes represent the ATs relevant to bloom days, and the red boxes represent the ATs relevant to non-bloom days. B0-1, the average AT on the day when the bloom was observed by satellite images (bloom day); B0-0, the average AT on the day when no bloom was observed by satellite images (non-bloom day); B4S-1, cumulative AT from the four days before the bloom day; B4S-0, cumulative AT from the four days before the non-bloom day; B7S-1, cumulative AT from the seven days before the bloom day; B7S-0, cumulative AT from the seven days before the non-bloom day

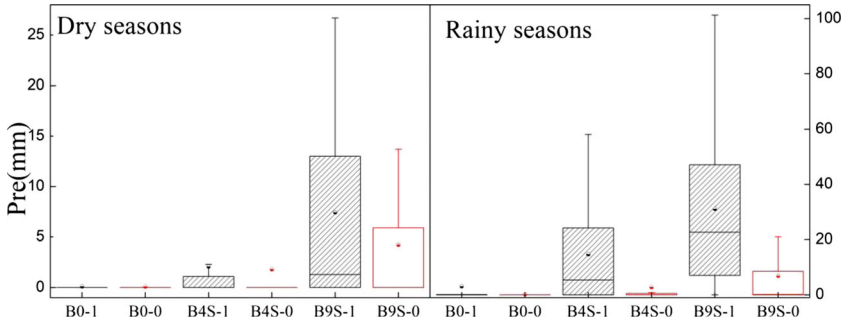

Fig. 15 Box plot of Pre in the short term. The black boxes represent the Pre relevant to bloom days, and the red boxes represent the Pre relevant to non-bloom days. B0-1, daily precipitation on the day when the bloom was observed by satellite images (bloom day); B0-0, daily precipitation on the day when no bloom was observed by satellite images (non-bloom day); B4S-1, cumulative precipitation from the four days before the bloom day; B4S-0, cumulative precipitation from the four days before the non-bloom day; B9S-1, cumulative precipitation from the nine days before the bloom day; B9S-0, cumulative precipitation from the nine days before the non-bloom day

nine days before October 10 to October 13 was 36.2 mm, 36.2 mm, 26.9 mm, and 26.9 mm, respectively (Case Oct), which was favorable for bloom formation.

In summary, monthly Pre and monthly average bloom area exhibited a statistically significant positive correlation. The suitable accumulation of Pre from the nine days before a bloom day was always more than 10 mm.

Conclusion

To overcome the shortage of effective images in Dianchi Lake, which is located in a rainy and cloudy area, HJ-1/CCD, GF-1/WFV, and Landsat-8/OLI data were used to generate a bloom record from 2009 to 2016. The area of the blooms extracted from different sensors using the VB-FAH index was consistent; thus, the use of multiple sensor data greatly improves the monitoring frequency of blooms.

The bloom area in Dianchi Lake varied considerably in space and time. Temporally, serious algae blooms occurred in 2011, 2013, and 2016, with higher frequency and size compared to other years. During a year, the frequencies of blooms had three peaks. The first appeared in April, followed by August and November. Spatially, the bloom coverage was first located in the northern part, then moved to the southern lake starting in July and then diffused to the entire lake.

The responses of bloom dynamics to meteorological factors were quantified based on the long-term bloom record. The results show that different meteorological factors have different effects on blooms at different timescales: AT in spring and SHs in summer were highly correlated with yearly bloom area ($r = -0.705$, $p = 0.05$ and $r = -0.737$, $p = 0.05$); the WS and SHs at a monthly timescale strongly affected the expansion and occurrence of blooms in the short term, and thereafter, they were highly correlated with ln(monthly average bloom area) ($r = -0.586$, $p = 0.01$ and $r = -0.551$, $p = 0.01$); precipitation had a great influence on the occurrence of blooms in the short term. Cyanobacteria blooms often erupted under low wind speed (2.35 ± 0.78 m/s in the dry season and 2.01 ± 0.75 m/s in the rainy season) and with suitable cumulative sunshine hours (48 h to 72 h in the dry season and 35 h to 57 h in the rainy season) and a sufficient amount of precipitation.

Funding information This study was supported by the National Key R&D Program of China (Grant No. 2017YFB0503902), the National Natural Science Foundation of China (Grant Nos. 41671340, 41701412, and 41701423), the Major Science and Technology Program for Water Pollution Control and Treatment (Grant No. 2017ZX07302-003), and the Natural Science Foundation of Jiangxi Province (Grant No. 20171BAB213024).

References

Allinger LE, Reavie ED (2013) The ecological history of Lake Erie as recorded by the phytoplankton community. J Great Lakes Res 39: 365–382

Bertani I, Obenour DR, Steger CE, Stow CA, Gronewold AD, Scavia D (2016) Probabilistically assessing the role of nutrient loading in harmful algal bloom formation in western Lake Erie. J Great Lakes Res 42:1184–1192

Brand LE, Compton A (2007) Long-term increase in Karenia brevis abundance along the Southwest Florida coast. Harmful Algae 6: 232–252

Cao H, Kong F, Luo L, Shi X, Yang Z, Zhang X, Tao Y (2006) Effects of wind and wind-induced waves on vertical phytoplankton distribution and surface blooms of Microcystis aeruginosa in Lake Taihu. J Freshw Ecol 21:231–238

Carey CC, Ibelings BW, Hoffmann EP, Hamilton DP, Brookes JD (2012) Eco-physiological adaptations that favour freshwater cyanobacteria in a changing climate. Water Res 46:1394–1407

Carmichael WW (2001) Health effects of toxin-producing cyanobacteria: "the CyanoHAB". Hum Ecol Risk Assess 7:1393–1407

Cloern JE, Schraga TS, Lopez CB, Knowles N, Grover Labiosa R, Dugdale R (2005) Climate anomalies generate an exceptional dinoflagellate bloom in San Francisco Bay. Geophys Res Lett 32

Cronberg, Gertrud, Claes (1981) Cyanodictyon imperfectum, a new chroococcal blue-green alga from Lake Trummen, Sweden 101–110

Cui T-W, Zhang J, Sun L-E, Jia Y-J, Zhao W, Wang Z-L, Meng J-M (2012) Satellite monitoring of massive green macroalgae bloom (GMB): imaging ability comparison of multi-source data and drifting velocity estimation. Int J Remote Sens 33:5513–5527

Davis CO, Kavanaugh M, Letelier R, Bissett WP, Kohler D (2007) Spatial and spectral resolution considerations for imaging coastal waters. Proc SPIE 6680

Francis G (1878) Poisonous Australian lake. Nature 18:11–12

Gao L, Zhou J-M, Yang H, Chen J (2005) Phosphorus fractions in sediment profiles and their potential contributions to eutrophication in Dianchi Lake. Environ Geol 48:835–844

Gerla DJ, Mooij WM, Huisman J (2011) Photoinhibition and the assembly of light-limited phytoplankton communities. Oikos 120:359–368

Guo W-H, Yu M, Liu Q-X, Wu J, Li X-G (2015) Vernalization process and the relationship between inductive low temperature in *Microcystis aeruginosa* in Dianchi Lake. Ecol Environ Sci 24(12): 2022–2026 **(in Chinese)**

Guo W-H, Liu Q-X, Peng X-W, Liu C-X (2016) Principle of vernalization in *Microcystis aeruginosa* in Dianchi Lake and improvement of gene model on controlling the vernalization. Ecol Environ Sci 25(12):2028–2034 **(in Chinese)**

Heisler J, Glibert P, Burkholder J, Anderson D, Cochlan W, Dennison W, Gobler C, Dortch Q, Heil C, Humphries E (2008) Eutrophication and harmful algal blooms: a scientific consensus. Harmful Algae 8: 3–13

Higgins SN, Pennuto CM, Howell ET, Lewis TW, Makarewicz JC (2012) Urban influences on Cladophora blooms in Lake Ontario. J Great Lakes Res 38:116–123

Ho JC, Stumpf RP, Bridgeman TB, Michalak AM (2017) Using Landsat to extend the historical record of lacustrine phytoplankton blooms: a Lake Erie case study. Remote Sens Environ 191:273–285

Hu C, Lee Z, Ma R, Yu K, Li D, Shang S (2010) Moderate resolution imaging spectroradiometer (MODIS) observations of cyanobacteria blooms in Taihu Lake, China J Geophys Res 115

Huang C, Wang X, Yang H, Li Y, Wang Y, Chen X, Xu L (2014) Satellite data regarding the eutrophication response to human activities in the plateau lake Dianchi in China from 1974 to 2009. Sci Total Environ 485-486:1–11

Huang C, Shi K, Yang H, Li Y, Zhu A, Sun D, Xu L, Zou J, Chen X (2015) Satellite observation of hourly dynamic characteristics of algae with Geostationary Ocean Color Imager (GOCI) data in Lake Taihu. Remote Sens Environ 159:278–287

Huang C, Zhang L, Li Y, Lin C, Huang T, Zhang M, A-x Z, Yang H, Wang X (2018) Carbon and nitrogen burial in a plateau lake during eutrophication and phytoplankton blooms. Sci Total Environ 616: 296–304

Huisman J, Sommeijer B (2002) Population dynamics of sinking phytoplankton in light-limited environments: simulation techniques and critical parameters. J Sea Res 48:83–96

JÖHnk KD, Huisman JEF, Sharples J, Sommeijer BEN, Visser PM, Stroom JM (2008) Summer heatwaves promote blooms of harmful cyanobacteria. Glob Chang Biol 14:495–512

Kahru M, Leppanen JM, Rud O (1993) Cyanobacterial blooms cause heating of the sea surface. Mar Ecol Prog Ser 101:1–7

Kanoshina I, Lips U, Leppänen J-M (2003) The influence of weather conditions (temperature and wind) on cyanobacterial bloom development in the Gulf of Finland (Baltic Sea). Harmful Algae 2:29–41

Kutser T (2004) Quantitative detection of chlorophyll in cyanobacterial blooms by satellite remote sensing. Limnol Oceanogr 49:2179–2189

Kutser T (2009) Passive optical remote sensing of cyanobacteria and other intense phytoplankton blooms in coastal and inland waters. Int J Remote Sens 30:4401–4425

Li M, Xie G, Lu W, Dai C (2011) Effect of meteorological conditions on blue algal bloom distribution in Dianchi Lake. J Meteorol Sci 31: 639–645 **(in Chinese)**

Li J, Chen X, Tian L, Huang J, Feng L (2015) Improved capabilities of the Chinese high-resolution remote sensing satellite GF-1 for monitoring suspended particulate matter (SPM) in inland waters: radiometric and spatial considerations. ISPRS J Photogramm Remote Sens 106:145–156

Lu W-K, Yu L, Ou X, Li F (2017) Relationship between occurrence frequency of cyanobacteria bloom and meteorological factors in Lake Dianchi. J Lake Sci 29:534–545 **(in Chinese)**

Ma X, Wang Y, Feng S, Wang S (2015) Vertical migration patterns of different phytoplankton species during a summer bloom in Dianchi Lake, China. Environ Earth Sci 74:3805–3814

Paerl HW, Huisman J (2008) Blooms like it hot. Science 320:57–58

Pan J, Wenchao amp LI, Chen K (2006) A study on the environmental effect in the zone of restoration of aquatic plants at the northeastern Dianchi Lake: II. The effect on removing the pollutants. J Lake Sci 18:578–584 **(in Chinese)**

Qin B, Xu P, Wu Q, Luo L, Zhang Y (2007) Environmental issues of Lake Taihu, China. Hydrobiologia 581:3–14

Reichwaldt ES, Ghadouani A (2012) Effects of rainfall patterns on toxic cyanobacterial blooms in a changing climate: between simplistic scenarios and complex dynamics. Water Res 46:1372–1393

Reynolds CS (2006): Ecology of phytoplankton. Cambridge University Press

Shaw G, Garnett C, Moore MR, Florian P (2001) The predicted impact of climate change on toxic algal (cyanobacterial) blooms and toxin production in Queensland. Environ Health 1:76

Sheng H, Liu H, Wang C, Guo H, Liu Y, Yang Y (2012) Analysis of cyanobacteria bloom in the Waihai part of Dianchi Lake, China. Ecol Inf 10:37–48

Shi K, Li Y, Li L, Lu H (2013) Absorption characteristics of optically complex inland waters: implications for water optical classification. J Geophys Res Biogeo 118:860–874

Shi K, Zhang Y, Li Y, Li L, Lv H, Liu X (2015a) Remote estimation of cyanobacteria-dominance in inland waters. Water Res 68:217–226

Shi K, Zhang Y, Zhu G, Liu X, Zhou Y, Xu H, Qin B, Liu G, Li Y (2015b) Long-term remote monitoring of total suspended matter concentration in Lake Taihu using 250 m MODIS-Aqua data. Remote Sens Environ 164:43–56

Shi K, Zhang Y, Zhou Y, Liu X, Zhu G, Qin B, Gao G (2017) Long-term MODIS observations of cyanobacterial dynamics in Lake Taihu: responses to nutrient enrichment and meteorological factors. Sci Rep 7:40326

Shi K, Zhang Y, Zhu G, Qin B, Pan D (2018) Deteriorating water clarity in shallow waters: evidence from long term MODIS and in-situ observations. Int J Appl Earth Obs Geoinf 68:287–297

Stumpf RP, Wynne TT, Baker DB, Fahnenstiel GL (2012) Interannual variability of cyanobacterial blooms in Lake Erie. PLoS One 7: e42444

Stumpf RP, Johnson LT, Wynne TT, Baker DB (2016) Forecasting annual cyanobacterial bloom biomass to inform management decisions in Lake Erie. J Great Lakes Res 42:1174–1183

Walsby AE (1994) Gas vesicles. Microbiol Rev 58:94

Wu T, Qin B, Brookes JD, Shi K, Zhu G, Zhu M, Yan W, Wang Z (2015) The influence of changes in wind patterns on the areal extension of surface cyanobacterial blooms in a large shallow lake in China. Sci Total Environ 518-519:24–30

Wu Y, Huang T, Huang C, Shen Y, Luo Y, Yang H, Yu Y, Li R, Gao Y, Zhang M (2018) Internal loads and bioavailability of phosphorus and nitrogen in Dianchi Lake, China. Chin Geogr Sci 28:851–862

Xie G, Li M, Lu W (2010) Spectral features, remote sensing identification and breaking-out meteorological conditions of algal bloom in Lake Dianchi. J Lake Sci 22:327–336 **(in Chinese)**

Xing Q, Hu C (2016) Mapping macroalgal blooms in the Yellow Sea and East China Sea using HJ-1 and Landsat data: application of a virtual baseline reflectance height technique. Remote Sens Environ 178: 113–126

Yang Z, Zhang M, Shi X, Kong F, Ma R, Yu Y (2016) Nutrient reduction magnifies the impact of extreme weather on cyanobacterial bloom formation in large shallow Lake Taihu (China). Water Res 103:302–310

Zhang M, Duan H, Shi X, Yu Y, Kong F (2012) Contributions of meteorology to the phenology of cyanobacterial blooms: implications for future climate change. Water Res 46:442–452

Zhang Y, Shi K, Liu J, Deng J, Qin B, Zhu G, Zhou Y (2016) Meteorological and hydrological conditions driving the formation and disappearance of black blooms, an ecological disaster phenomena of eutrophication and algal blooms. Sci Total Environ 569-570: 1517–1529

Zheng Z, Li Y, Guo Y, Xu Y, Liu G, Du C (2015) Landsat-based long-term monitoring of total suspended matter concentration pattern change in the wet season for Dongting Lake, China. Remote Sens 7:13975–13999

Zhou M-J, Zhu M-Y (2006) Progress of the project "Ecology and Oceanography of Harmful Algal Blooms in China". Advances in Earth Sci 21:673–679

Zhou Q, Zhang Y, Lin D, Shan K, Luo Y, Zhao L, Tan Z, Song L (2016) The relationships of meteorological factors and nutrient levels with phytoplankton biomass in a shallow eutrophic lake dominated by cyanobacteria, Lake Dianchi from 1991 to 2013. Environ Sci Pollut Res Int 23:15616–15626